Optically Detected Triplet-State Magnetic Resonance Studies of the DNA Complexes of the Bisquinoline Analogue of Echinomycin†

Thomas V. Alfredson,‡,§ August H. Maki,*,‡ and Michael J. Waring‖

Chemistry Department, University of California, Davis, California 95616, and Pharmacology Department, University of Cambridge, Tennis Court Road, Cambridge CB2 1QJ, U.K.

Received May 3, 1991; Revised Manuscript Received July 16, 1991

ABSTRACT: The polymeric DNA and model duplex oligonucleotide complexes of the bisquinoline analogue of echinomycin (2QN) have been studied by optical detection of triplet-state magnetic resonance (ODMR) spectroscopy, with the quinoline chromophores of the drug used as intrinsic probes. Plots of ODMR transition frequencies versus monitored wavelength revealed heterogeneity in the phosphorescence emission of 2QN which was ascribed to the presence of a major and minor conformation of the drug in aqueous solutions (referred to as the red and blue forms of 2QN, respectively, in this report). ODMR results, in conjunction with findings from low-temperature phosphorescence investigations, indicate that the quinoline chromophores of the major (red) form of 2QN are involved in aromatic stacking interactions in complexes with the natural DNAs from *Escherichia coli*, *Micrococcus lysodeikticus*, *Clostridium perfringens*, and calf thymus as evidenced by red shifts in the phosphorescence 0,0-band of the drug, reductions in the phosphorescence lifetime and zero-field splitting (zfs) *D* and *E* parameters, and polarity reversals of the ODMR slow passage signals upon complex formation between the analogue and DNA. The polarity reversals, which reflect shifts in the triplet-state sublevel populations induced by complex formation, apparently result from changes in the triplet sublevel decay constants upon binding to the natural DNAs. The 2QN complexes of the double-stranded alternating copolymers poly(dG-dC)·poly(dG-dC) [abbreviated as poly[d(G-C)$_2$]] and poly(dA-dT)·poly(dA-dT) [abbreviated as poly[d(A-T)$_2$], the homopolymer duplexes poly(dG)·poly(dC) [abbreviated as poly(dG·dC)] and poly(dA)·poly(dT) [abbreviated as poly(dA·dT)], and the self-complementary oligonucleotides d(ACGT)$_2$, d(TCGA)$_2$, and d(ACGTACGT)$_2$ were also investigated. The extent of reduction of the zfs *D* parameter (ΔD) for the major form of 2QN upon complex formation with the polymeric DNAs was found to scale linearly with the standard free energy of the drug–DNA interaction ($\Delta G°$) calculated from previously reported binding studies for these targets [Fox, K. R., et al. (1980) *Biochem. J. 191*, 729–740]. This relationship between spectroscopic and thermodynamic properties of the 2QN–polynucleotide complexes is a consequence of the effects of base stacking interactions on the electronic states of the intercalator, which were postulated to arise from second-order shifts of the ground-state and the triplet-state energies of the complex on the basis of a modification of the solvent effect theory of van Egmond et al. [(1975) *Chem. Phys. Lett. 34*, 423–426].

Two classes of cyclic depsipeptide antibiotics, the quinomycins and the triostins, occur as natural products of several species of *Streptomyces* (Wakelin, 1986). They contain, in common, two quinoxaline moieties that are attached by amide linkages to a pair of serine residues of the depsipeptide ring. The most frequently studied members of the quinomycin and triostin classes are echinomycin and triostin A, respectively. They differ only in the structure of the group that forms a ring cross-bridge which consists of a thioacetal and a simple disulfide, respectively. Echinomycin (Figure 1) and triostin A were proposed to bind to duplex DNA by a bisintercalation mode, on the basis of their interaction with superhelical DNA (Waring & Wakelin, 1974; Wakelin & Waring, 1976). This binding mode, in which the peptide ring binds to the minor groove and the quinoxaline residues sandwich two base pairs, has been confirmed by single-crystal X-ray diffraction of oligonucleotide complexes (Wang et al., 1984; Ughetto et al., 1985; Quigley et al., 1986). Footprinting studies (Low et al., 1984; Van Dyke & Dervan, 1984) demonstrate the preference of echinomycin for binding to CpG steps in the nucleotide sequence and suggest a minimum binding site size of four base pairs, with the strongest binding occurring with ACGT and TCGT sequences. NMR studies of echinomycin bisintercalation complexes with oligonucleotides (Gao & Patel, 1988) produced evidence of stacking interactions between quinoxaline rings of the drug and A·T base pairs flanking the CpG intercalation site, in agreement with crystal structure findings.

In a recent study (Alfredson & Maki, 1990) optical detection of magnetic resonance (ODMR)[1] was used to investigate the effects of echinomycin complexing with several DNAs on the triplet-state properties of the phosphorescent

† This research was partially supported by NIH Grant ES-02662 and by grants from the University of California, Davis, Committee on Research, the Cancer Research Campaign, and the Royal Society.

‡ University of California.

§ Present address: Syntex Research, 3401 Hillview Rd., Palo Alto, CA 94304.

‖ University of Cambridge.

[1] Abbreviations: *D* and *E*, triplet-state zero-field splitting parameters; DNA, deoxyribonucleic acid; EDTA, ethylenediaminetetraacetic acid; HPLC, high-performance liquid chromatography; LPSE, buffer consisting of 2 mM phosphate, 10 mM NaCl, and 0.1 mM EDTA at pH 7; NMR, nuclear magnetic resonance; MIDP, microwave-induced delayed phosphorescence; ODMR, optical detection of triplet-state magnetic resonance; OPC, oligonucleotide purification cartridges; poly(dA·dT), double helix formed by the two homopolymers poly(dA) and poly(dT); poly[d(A-T)$_2$], double helix formed by two chains of alternating A's and T's; poly(dG·dC), double helix formed by the two homopolymers poly(dG) and poly(dC); poly[d(G-C)$_2$], double helix formed by two chains of alternating G's and C's; Trp, tryptophan; 2QN, the bisquinoline analogue of echinomycin; zfs, zero-field spliting.

0006-2960/91/0430-9665$02.50/0

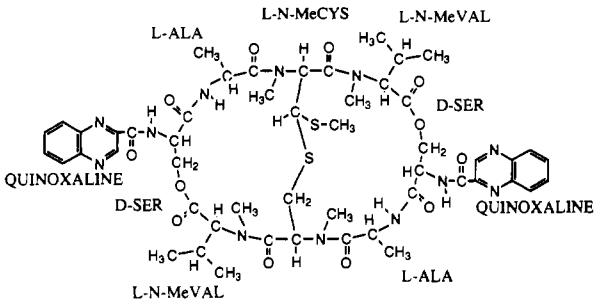

ECHINOMYCIN

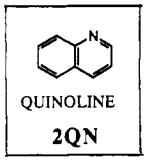

FIGURE 1: Structure of echinomycin. In the bisquinoline derivative of echinomycin, 2QN, both quinoxaline rings are replaced by quinoline rings (see inset).

quinoxaline residue. This work revealed that echinomycin and its complexes with oligo- and polynucleotides were heterogeneous, consisting of a minor and a major form; the phosphorescence of the minor form is shifted to the blue relative to that of the major form. These forms of echinomycin have been referred to as the blue and red forms of the drug, respectively. We have attributed them tentatively to rotational conformers of quinoxaline with respect to the amide linkage with the cyclic peptide. Both the blue and red forms bind to DNA as evidenced by changes in the quinoxaline triplet-state zero-field splittings (zfs). In addition, triplet-state sublevel lifetimes of the red form are affected by binding, leading to the reversal of ODMR signal polarity in some DNA complexes. The zfs changes of the major (red) form of echinomycin were found to correlate with the binding constants measured for various DNA targets by Wakelin and Waring (1976), but no correlation was found for the minor (blue) form. The observed binding constant, of course, is influenced most strongly by the major form of the antibiotic which is present.

Initial investigations of biosynthetic replacement of the chromophores in echinomycin by Yoshida et al. (1968) demonstrated the feasibility of this technique for producing novel quinomycin derivatives. In these early studies, quinaldic acid was used as an analogue of the naturally occurring quinoxaline-2-carboxylic acid of the *Streptomyces*. Subsequent directed biosynthesis efforts (Fox et al., 1980; Cornish et al., 1983; Gauvreau & Waring, 1984) have produced a large variety of novel echinomycin derivatives. Previous work on 2QN, which differs from echinomycin in that each quinoxaline chromophore is replaced with quinoline, has demonstrated that this derivative apparently interacts with DNA via a bisintercalation mode, but with binding specificities that differ greatly from those of the parent drug (Fox et al., 1980). For example, 2QN exhibits binding constants for the alternating copolymers, poly[d(G-C)$_2$] and poly[d(A-T)$_2$], that are nearly an order of magnitude larger than the respective binding constants of echinomycin. These results suggest that changes in the intercalating chromophores, even subtle ones, can influence significantly the sequence specificity and stability of DNA binding. In order to examine further these effects of chromophore substitution, we have investigated, using ODMR spectroscopy, the complexes of 2QN with various DNA targets, including the oligonucleotide duplexes d(ACGT)$_2$, d(TCGA)$_2$, and d(ACGTACGT)$_2$, the double-stranded alternating copolymers poly[d(G-C)$_2$] and poly[d(A-T)$_2$], the homopolymer duplexes poly(dG·dC) and poly(dA·dT), and the natural DNAs from *Escherichia coli*, *Micrococcus lysodeikticus*, *Clostridium perfringens*, and calf thymus. The results which we report here, when combined with those presented previously (Alfredson & Maki, 1990), suggest that for the major (red) form of both echinomycin and 2QN the reduction in the zfs D parameter, $-\Delta D$, of the intercalating chromophore scales linearly with the standard free energy of the drug–DNA interaction, $-\Delta G°$. Consequently, measurement of the zfs changes of the chromophore upon binding to various sequences of DNA can be used to assess the contribution of aromatic stacking interactions to the stability and, possibly, specificity of binding.

Experimental Procedures

Sample Preparation. The 2QN peptide was prepared by using directed biosynthesis (Gauvreau & Waring, 1984). The crude peptide, which contained 1QN and echinomycin, was purified by using reversed-phase HPLC prior to spectroscopic investigation as described previously (Alfredson et al., 1990). Binding of 2QN to DNA was carried out in a manner similar to that utilized for the echinomycin investigations (Alfredson & Maki, 1990) using LPSE buffer (2 mM KH_2PO_4, 10 mM NaCl, 0.01 mM EDTA at pH 7). Double-stranded poly[d(A-T)$_2$], poly[d(G-C)$_2$], poly(dA·dT), and poly(dG·dC) were obtained from Pharmacia, Piscataway, NJ. Calf thymus (highly polymerized sodium salt, type 1), *M. lysodeikticus*, *E. coli*, and *C. perfringens* DNAs were obtained from Sigma, St. Louis, MO. The polynucleotides were used without further purification. The duplex oligonucleotides d(ACGT)$_2$, d(TCGA)$_2$, and d(ACGTACGT)$_2$ were prepared on a Model 380 DNA synthesizer (Applied Biosystems, Foster City, CA) and subsequently deprotected and purified by means of OPC purification cartridges (Applied Biosystems, Inc.) following standard procedures. Oligonucleotide purity was at least 95% as determined by HPLC analysis.

Binding of 2QN to the natural and synthetic DNAs was carried out by means of a modified solid-shake procedure (Lee & Waring, 1978), as described previously (Alfredson & Maki, 1990). The concentration of bound drug was measured spectrophotometrically by using the weak absorption band of 2QN at 315 nm. Generally, 90–95% of 2QN in solution was bound to the DNA. Ethylene glycol (EG) (16% v/v) was added as a cryosolvent immediately prior to low-temperature phosphorescence and ODMR measurement.

Phosphorescence and ODMR Spectroscopic Methods. Procedures and equipment used for obtaining phosphorescence spectra at 77 and 4.2 K and slow passage ODMR spectra at 1.2 K were the same as described previously (Alfredson & Maki, 1990). Phosphorescence decays obtained at 77 K were analyzed as described previously (Maki & Co, 1976). Microwave-induced delayed phosphorescence (MIDP) (Schmidt et al., 1971) was employed at 1.2 K to obtain individual sublevel lifetimes. Details of this procedure have been described recently (Alfredson & Maki, 1990).

Results

Phosphorescence and ODMR of 2QN and Quinoline. Figure 2 displays the phosphorescence spectra at 4.2 K of quinoline and 2QN in LPSE buffer with 16% EG. Quinoline yields an emission profile that exhibits a well-resolved vibronic manifold with a 0,0-band maximum of 457.3 nm. In contrast, a less well-resolved emission profile is obtained from 2QN with an apparent 0,0-band maximum at 480.5 nm. The overall vibronic structure is quite similar to that of quinoline. Previous

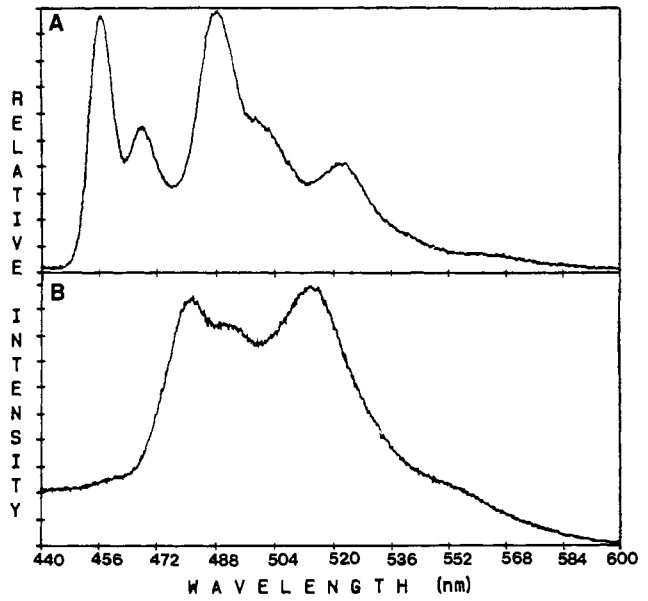

FIGURE 2: Phosphorescence emission spectra at 4.2 K of (A) quinoline, 80 μM, and (B) 2QN, 15 μM, in LPSE buffer with 16% EG. Excitation was at 313 nm.

work on Trp residues in proteins (von Schütz et al., 1974; Kwiram et al., 1978; Tsao et al., 1989) and quinoxaline in echinomycin (Alfredson & Maki, 1990) has shown that heterogeneity in chromophore phosphorescence can be detected by a combination of optical wavelength selection and ODMR. By observing ODMR signals through a monochromator using a narrow band-pass, a discontinuity in the plot of ODMR frequency vs monitored wavelength is indicative of multiple sites provided only a single vibronic band is monitored. Heterogeneity detected by this means was found in echinomycin (Alfredson & Maki, 1990) and attributed to distinct conformations that give rise to blue- and red-shifted phosphorescence spectra. The results of wavelength-selected ODMR experiments carried out on the phosphorescent states of quinoline and 2QN are given in Figure 3. In quinoline, only the T_z sublevel is detectably radiative, and thus, provided spin–lattice relaxation is quenched, only the $D + E$ and $2E$ ODMR signals are visible. For quinoline, the z-axis is the principal in-plane zfs axis which lies closest (within ca. ±13°) to the long axis of the molecule (Vincent & Maki, 1965), while x is the out-of-plane axis. Both signals occur with negative polarity in methanol and LPSE buffer, reflecting a larger steady-state population in the T_z sublevel than in the (T_x, T_y) sublevels. The lack of discontinuity in the ODMR frequency vs wavelength plot is consistent with an effectively continuous distribution of solvent environments. On the other hand, 2QN produces all three ODMR signals in methanol and LPSE buffer, apparently the consequence of at least two detectably radiative sublevels in the triplet state of the quinoline-2-carboxamide moieties of the peptide. As in quinoline, the $2E$ signal has negative polarity, while the $D + E$ signal has either positive or negative polarity, depending on the solvent and detection wavelength (see below). In contrast to the behavior of quinoline, a discontinuity at ca. 477 nm in the wavelength-dependent ODMR behavior of 2QN dissolved in LPSE buffer (Figure 3) reveals the presence of what are apparently two conformations that give rise to a blue-shifted (minor) and a red-shifted (major) phosphorescence spectrum, respectively. Both the $2E$ and $D + E$ signals have negative polarity throughout. This behavior is similar to that found earlier in echinomycin (Alfredson & Maki, 1990). A similar discontinuity occurs at ca. 475 nm for 2QN in methanol solvent (data

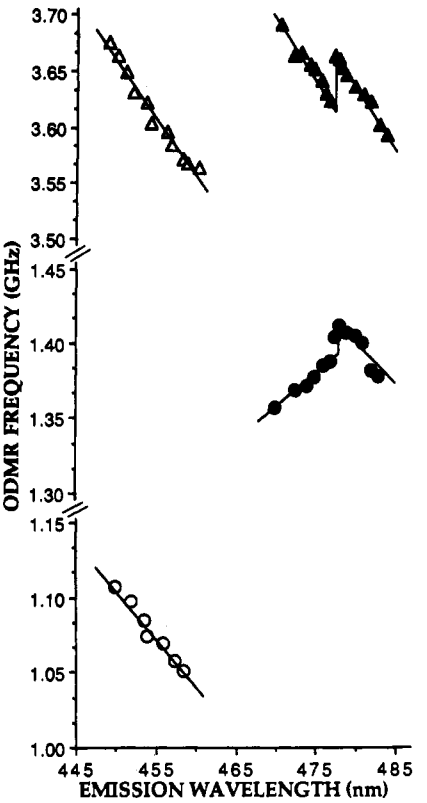

FIGURE 3: ODMR frequency versus emission wavelength for 2QN and quinoline at 1.2 K. Emission slits were set at 1.5-nm band-pass. Microwave sweep rate was 310 MHz/s (uncorrected for rapid passage effects). (○) Quinoline $2E$ signal; (●) 2QN $2E$ signal; (△) quinoline $D + E$ signal; (▲) 2QN $D + E$ signal.

not shown). In this solvent, however, the $D + E$ ODMR signals to the blue of the discontinuity have positive polarity while those to the red are negative. Thus, as with echinomycin, ODMR signals from the blue triplet state of 2QN in LPSE buffer were obtained by monitoring the phosphorescence to the blue of this discontinuity (ca. 476 nm), and those from the red triplet state were obtained by monitoring the phosphorescence at the 0,0-band peak.

The triplet-state ODMR frequencies, zfs parameters (D and E), and the phosphorescence decay kinetics of the blue and red triplet states of 2QN are compared with those of quinoline in Table I. The red triplet state of 2QN has a smaller D and larger E than the blue triplet state. Both 2QN triplet states have a reduced D and an increased E relative to quinoline. A similar pattern is observed for echinomycin when it is compared with the parent chromophore, quinoxaline (Alfredson & Maki, 1990). This effect probably is due to electron delocalization into the carboxamide group at the 2-position of the chromophore.

Oligonucleotide–2QN Complexes. A significant red shift (5–6 nm) of the phosphorescence 0,0-band of 2QN is observed upon binding of the peptide to each of the oligonucleotides. ODMR signals were acquired for the blue and red triplet states of the bound drug by monitoring the phosphorescence at 476 nm and at the 0,0-band maximum, respectively. The properties of the blue and red triplet states of 2QN and its oligonucleotide complexes are summarized in Tables II and III, respectively. For the blue triplet state, the observed ODMR signals are of negative polarity. For the red triplet state, on the other hand, the $2E$ and $D + E$ signals are found to have positive polarity. Both D and E are found to decrease upon binding of 2QN to the oligonucleotides. A reduction in the zfs is consistent with stacking interactions which reduce the dipolar coupling of the

Table I: Triple-State Properties of 2QN and Quinoline in Aqueous Solution[a]

sample	phosphorescence decay[b] (s)	zero-field ODMR frequencies[c] (GHz)			zero-field splitting parameters[d] (GHz)	
		$2E$	$D-E$	$D+E$	D	E
2QN						
λ_{em} = 476 nm (blue)	0.10 (12) 0.43 (24) 1.07 (64)	1.300		3.601	2.951 (±0.014)	0.650 (±0.009)
$\lambda_{0,0}$ = 481 nm (red)	0.09 (8) 0.45 (26) 1.00 (66)	1.343	2.240 (+)	3.570	2.898 (±0.011)	0.672 (±0.009)
quinoline						
$\lambda_{0,0}$ = 456.3 nm	0.84 (3) 1.27 (97)	1.018		3.616	3.107	0.509

[a] Sample concentrations were 30 μM 2QN and 80 mM quinoline in LPSE buffer containing 16% ethylene glycol. Excitation was at 313 nm with emission wavelengths measured at 4.2 K. [b] Decay measurements were made at 77 K and fit to a multicomponent exponential with the preexponential contributions (%) listed in parentheses for each lifetime component. Standard deviation for the lifetime measurements was 0.02 s (n = 5). [c] Zero-field ODMR frequencies were measured at 1.2 K and corrected for rapid passage effects. Signals are all of negative polarity except where indicated by (+). [d] Standard deviations for 2QN calculated from n = 4 independent measurements are listed in parentheses. The standard deviation of the mean is less by $1/\sqrt{n}$.

Table II: Triplet-State Properties of 2QN–Oligonucleotide Complexes: Blue Triplet State of 2QN[a]

sample	ODMR signals[b] (GHz)		zero-field splitting parameters (GHz)		ΔD[c] (MHz)
	$2E$	$D+E$	D	E	
2QN	1.300	3.601	2.951 (±0.014)	0.650 (±0.009)	
2QN–d(ACGT)$_2$	1.323	3.586	2.924	0.662	−27
2QN–d(TCGA)$_2$	1.353	3.640	2.963	0.677	+12
2QN–d(ACGTACGT)$_2$	1.337	3.525	2.856	0.669	−95

[a] Samples were dissolved in LPSE buffer with 16% ethylene glycol. Excitation was at 313 nm, and emission was monitored at 476 nm. [b] Zero-field ODMR frequencies were measured at 1.2 K and are corrected for rapid passage effects. All signals have negative polarity. [c] Shift of zfs D value upon binding to oligonucleotide targets.

Table III: Triple-State Properties of 2QN–Oligonucleotide Complexes: Red Triplet State of 2QN[a]

sample	$\lambda_{0,0}$ (nm)	phosphorescence decay[b] (s)	ODMR signals[c] (GHz)			zero-field splitting parameters (GHz)		ΔD[d] (MHz)
			$2E$	$D-E$	$D+E$	D	E	
2QN	481.0	0.09 (8) 0.45 (26) 1.00 (66)	1.343	2.240 (+)	3.570	2.898 (±0.010)	0.672 (±0.005)	
2QN–d(ACGT)$_2$	486.0	0.03 (8) 0.22 (24) 0.86 (68)	1.154 (+)	2.251 (+)	3.433 (+)	2.856	0.577	−42
2QN–d(TCGA)$_2$	485.4	0.03 (12) 0.29 (30) 0.97 (58)	1.150 (+)	2.261 (+)	3.438 (+)	2.863	0.575	−35
2QN–d(ACGTACGT)$_2$	486.8	0.03 (7) 0.22 (29) 0.85 (64)	1.218 (+)	2.229 (+)	3.436 (+)	2.827	0.609	−71

[a] Samples were dissolved in LPSE buffer containing 16% ethylene glycol. Excitation was at 313 nm, and 0,0-band peak wavelengths were recorded at 4.2 K. [b] Decays were measured at 77 K and fit to a multicomponent exponential with preexponential contributions (%) listed in parentheses for each lifetime component. [c] Zero-field ODMR frequencies were measured at 1.2 K and corrected for rapid passage effects. (+) indicates that a positive polarity ODMR signal was observed. [d] Change in zfs D value upon binding to oligonucleotide targets.

unpaired electrons whose wave function expands in a more polarizable environment. The ODMR signals of the 2QN red triplet state are compared with those of the red triplet state of 2QN–d(ACGTACGT)$_2$ and 2QN–(TCGA)$_2$ complexes in Figure 4.

2QN–Polynucleotide Complexes. The phosphorescence spectra of several polynucleotide–2QN complexes in aqueous buffer are compared in Figure 5. These spectra show a red shift of the 0,0-band relative to 2QN. The largest shift, ca. 8 nm, is exhibited by the 2QN–poly[d(G-C)$_2$] complex, while the smallest ones, ca. 1.5 nm, are given by the 2QN complexes with poly(dA·dT) and poly[d(A-T)$_2$]. The vibronic structure of the latter complex is particularly well resolved, suggesting a relatively homogeneous distribution of environments. The natural DNA complexes give intermediate red shifts of the 0,0-bands. The ODMR signals of the red triplet states of several polynucleotide–2QN complexes, obtained by monitoring the emission at the 0,0-band peak wavelength, are shown in Figure 6. Both the $2E$ and $D+E$ signals exhibit a decrease in frequency and a reversal in signal polarity upon complex formation with each of the polynucleotides with the exception of the 2QN–poly(dA·dT) complex whose ODMR spectrum closely resembles that of the free peptide. The negative component which can be seen on the high-frequency edge of the 2QN–poly[d(A-T)$_2$] complex arises from the significantly enhanced $D+E$ signal of the blue triplet state of the complex which could not be eliminated completely by wavelength selection. The ODMR spectra of the other natural DNA complexes resemble that of the *E. coli* DNA which is shown in Figure 6. The phosphorescence characteristics and ODMR frequencies of the blue and red triplet states of these complexes are listed in Tables IV and V, respectively, along with the zfs

Table IV: Triplet-State Properties of 2QN–Polymeric DNA Complexes: Blue Triplet State of 2QN[a]

sample	phosphorescence decay[b] (s)	ODMR signals[c] (GHz)		zero-field splitting parameters (GHz)		ΔD[d] (MHz)
		$2E$	$D + E$	D	E	
2QN	0.10 (12) 0.43 (24) 1.07 (64)	1.300	3.601	2.951 (±0.014)	0.650 (±0.009)	
2QN–poly(dA·dT)	0.09 (16) 0.36 (33) 1.08 (51)	1.323	3.645	2.983	0.662	+32
2QN–poly[d(G-C)$_2$]	0.08 (24) 0.49 (35) 1.14 (41)	1.425	3.622	2.909	0.713	−42
2QN–poly[d(A-T)$_2$]	0.10 (11) 0.44 (31) 0.99 (58)	1.205	3.560	2.957	0.603	+6
2QN–*M. lysodeikticus* DNA	0.09 (16) 0.36 (39) 1.06 (45)	1.314	3.526	2.869	0.657	−82
2QN–*E. coli* DNA	0.08 (6) 0.51 (18) 0.97 (76)	1.291	3.528	2.882	0.646	−69
2QN–calf thymus DNA	0.07 (7) 0.61 (21) 1.01 (72)	1.308	3.557	2.903	0.654	−48
2QN–*C. perfringens* DNA	0.07 (4) 0.39 (10) 1.02 (86)	1.283	3.525	2.883	0.642	−68

[a] Samples dissolved in LPSE buffer containing 16% ethylene glycol. Excitation was at 313 nm; emission was monitored at 476 nm. [b] Decay was measured at 77 K and fit to a multicomponent exponential with preexponential contributions (%) listed in parentheses for each lifetime component. [c] Zero-field ODMR frequencies were measured at 1.2 K and corrected for rapid passage effects. All signals have negative polarity. [d] Change in zfs D value upon binding to DNA targets.

Table V: Triplet-State Properties of 2QN–Polymeric DNA Complexes: Red Triplet State of 2QN[a]

sample	$\lambda_{0,0}$ (nm)	phosphorescence decay[b] (s)	ODMR signals[c] (GHz)			zero-field parameters (GHz)		ΔD[d] (MHz)	K_0[e] (μM^{-1})
			$2E$	$D - E$	$D + E$	D	E		
2QN	481.0	0.09 (8) 0.45 (26) 1.00 (66)	1.343	2.240 (+)	3.570	2.898 (±0.011)	0.0672 (±0.005)		
2QN–poly(dG·dC)	485.0	0.02 (24) 0.37 (20) 0.90 (56)	1.188 (+)	2.215 (+)	3.398 (+)	2.804	0.594	−94	NA
2QN–poly(dA·dT)	482.4	0.09 (13) 0.38 (24) 0.96 (63)	1.321	2.227 (+)	3.561	2.900	0.661	+2	NA
2QN–poly[d(G-C)$_2$]	488.8	0.05 (4) 0.39 (18) 0.83 (78)	1.270 (+)	2.181 (+)	3.430 (+)	2.795	0.635	−103	3.6
2QN–poly[d(A-T)$_2$]	482.6	0.10 (6) 0.45 (23) 0.89 (71)	1.298 (+)	2.140	3.422 (+)	2.773	0.649	−125	5.6
2QN–*M. lysodeikticus* DNA	485.4	0.06 (4) 0.34 (17) 0.88 (79)	1.150 (+)	2.240 (+)	3.402 (+)	2.827	0.575	−71	1.1
2QN–*E. coli* DNA	485.2	0.07 (2) 0.41 (10) 0.85 (88)	1.170 (+)	2.226 (+)	3.414 (+)	2.829	0.585	−69	1.7
2QN–calf thymus DNA	485.0	0.30 (10) 0.86 (90)	1.180 (+)	2.235 (+)	3.435 (+)	2.845	0.590	−54	1.0
2QN–*C. perfringens* DNA	484.4	0.49 (12) 0.89 (88)	1.173 (+)	2.285 (+)	3.458 (+)	2.871	0.587	−27	0.4

[a] Samples were dissolved in LPSE buffer with 16% ethylene glycol. Excitation was at 313 nm. [b] Decay was measured at 77 K and fit to a multicomponent exponential with preexponential contributions (%) listed in parentheses for each lifetime component. [c] Zero-field ODMR signals were measured at 1.2 K and corrected for rapid passage effects. Signals have negative polarity unless indicated by (+). [d] Change in D value upon binding to DNA targets. [e] Binding constants taken from Fox et al. (1980). Binding to the homopolymer duplexes was not measured.

parameters, D and E. The average equilibrium constants for 2QN binding to the various DNAs obtained from solvent partitioning and fluorescence quenching (Fox et al., 1980) are listed in Table V, as well. The complex 2QN–poly(dG·dC) is unique in exhibiting an intense very blue-shifted (ca. 80 nm) phosphorescence in addition to the "normal" one produced by 2QN and the other DNA complexes. The 77 K lifetime of the blue-shifted component is ca. 14 ms, considerably shorter than the ca. 1-s lifetime of the "normal" 2QN phosphorescence. The origin of the dual phosphorescence, which is only observed in the presence of 2QN, is currently under investigation.

The sublevel decay constants of the red triplet state of the 2QN–polynucleotide complexes are compared with those of 2QN in Table VI. The effect of complex formation on the individual decay constants of 2QN is analogous to those observed previously for echinomycin (Alfredson & Maki, 1990). In most cases, binding to DNA produces a significant increase in k_z, while k_x and k_y are reduced. As with echinomycin, these

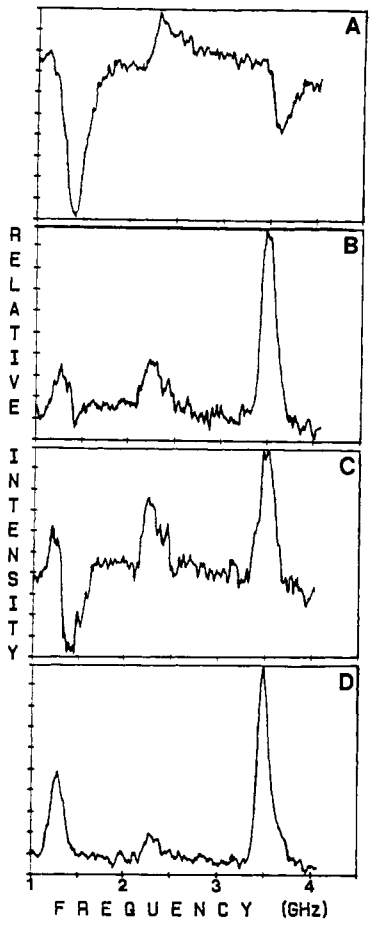

FIGURE 4: ODMR spectra of 2QN–oligonucleotide complexes: Red triplet state of 2QN. Excitation was at 313 nm; emission was monitored at the 0,0-band apex. Microwave sweep rate was 375 MHz/s; T = 1.2 K. (A) 2QN, 15 μM, in LPSE buffer with 16% EG; (B) 2QN–d(ACGT)$_2$ complex; (C) 2QN–d(TCGA)$_2$ complex; (D) 2QN–d(ACGTACGT)$_2$ complex. Approximate concentrations of the 2QN–DNA complexes ranged from 110 to 240 μM based on the concentration of the bound ligand.

Table VI: Triplet-State Kinetics of the DNA Complexes of the Major (Red) Form of 2QN[a]

sample	sublevel decay rates (s^{-1})[b]		
	k_x	k_y	k_z
2QN	0.34 (±0.05)	0.51 (±0.07)	1.9 (±0.3)
2QN–poly[d(G-C)$_2$]	0.30	0.40	3.0
2QN–poly[d(A-T)$_2$]	0.25	0.36	2.9
2QN–poly(dA·dT)	0.39	0.53	2.2
2QN–*M. lysodeikticus* DNA	0.24	0.38	2.9
2QN–*E. coli* DNA	0.27	0.46	3.2
quinoline			
in LPSE buffer	0.29	0.44	1.6
in durene[c]	0.19	0.32	3.1

[a] Samples dissolved in LPSE buffer containing 16% ethylene glycol. Excitation was at 313 nm, and emission was monitored at wavelengths slightly to the red of the apparent 0,0-band maximum. [b] The $k_u(u=x,y,z)$ values are apparent total decay rate constants obtained from MIDP measurements at 1.2 K. Standard deviations from 2QN calculated from n = 3 independent measurements are listed in parentheses. [c] Data from Schmidt et al. (1971).

changes correlate with polarity reversals of the $2E$ and $D + E$ transitions. It should be noted that the 2QN–poly(dA·dT) complex shows neither polarity reversals nor significant changes in the k's.

Although we have reported ODMR data for the blue triplet state of 2QN and its complexes, we will not discuss them in detail here since the blue form is a minor form of the drug and, as with echinomycin, the properties of the blue triplet state were found not to correlate with equilibrium constants for 2QN

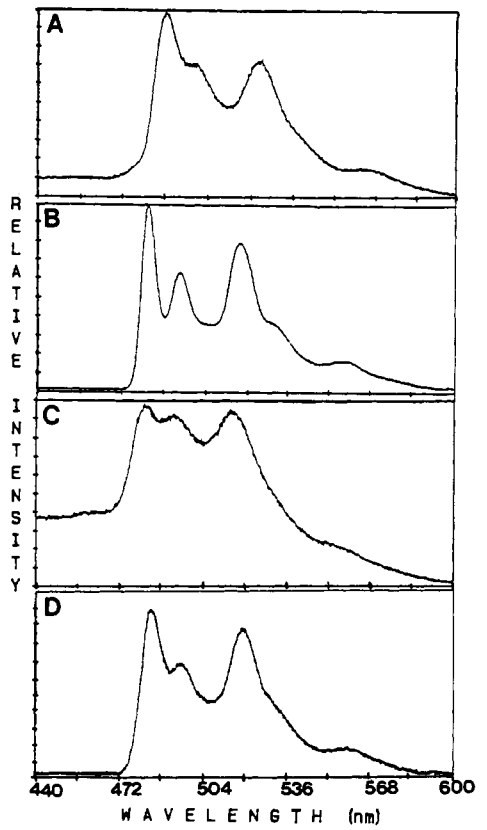

FIGURE 5: Phosphorescence spectra of 2QN–polynucleotide complexes. Excitation is at 313 nm; T = 4.2 K. (A) 2QN–poly[d(G-C)$_2$] complex; (B) 2QN–poly[d(A-T)$_2$] complex; (C) 2QN–poly(dA·dT) complex; (D) 2QN–*E. coli* DNA complex. Concentrations of the 2QN–DNA complexes ranged from approximately 100 to 300 μM.

binding to the various DNAs. The thermodynamic properties reflect to a large extent the major (red) form of the drug and its DNA complexes. For the blue triplet-state form of 2QN, D decreases significantly (between −40 and −80 MHz) upon binding to each of the polynucleotides listed in Table IV, except for poly(dA·dT) and poly[d(A-T)$_2$], which exhibit small increases in D. The E parameter is hardly affected except upon binding to the alternating copolymers; E increases by 60 MHz upon binding to poly[d(G-C)$_2$] while it decreases by −50 MHz when it binds to poly[d(A-T)$_2$]. Reliable data on the blue triplet state of the 2QN–poly(dG·dC) complex were not accessible because of interference from the intense blue component of the dual phosphorescence noted above. In contrast with the red triplet-state form of 2QN, the blue form did not exhibit polarity reversals of the $2E$ and $D + E$ ODMR signals when complexed with the polynucleotides. These signals maintained their negative polarity.

Figure 7 shows a plot of the change in the zfs D parameter (ΔD) of the red triplet state of 2QN vs. the drug–DNA binding free energies ($\Delta G°$) for the 2QN–polymeric DNA complexes calculated from the intrinsic association constants measured at ambient temperatures (Fox et al., 1980). The data fit a linear regression with a correlation coefficient of r = 0.99. Correlations between the thermodynamics of drug binding and the zfs data obtained from ODMR measurements on the red form of 2QN will be discussed in the following section.

Discussion

Triplet-State Properties of 2QN in Aqueous Solutions. Due to the extremely low solubility (ca. 2 μM) of 2QN in water, a trait in common with echinomycin, structural studies of the unbound drug in aqueous solvents have not been reported to

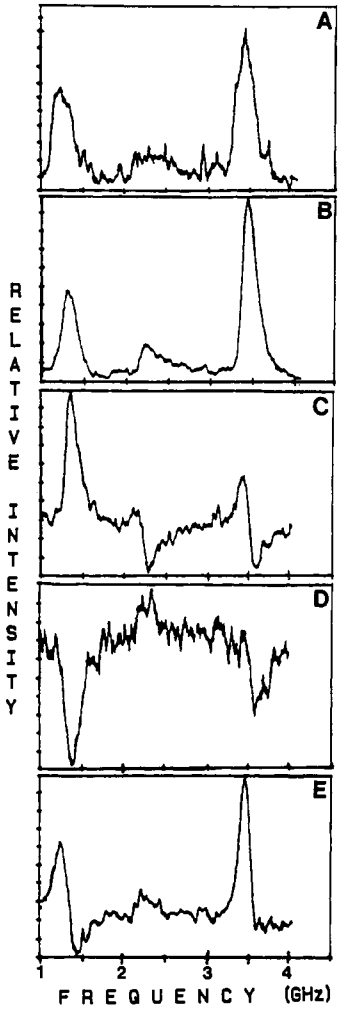

FIGURE 6: ODMR spectra of 2QN–polynucleotide complexes: 2QN red triplet state. Excitation was at 313 nm; emission was monitored at the 0,0-band peak. Microwave sweep rate was 375 MHz/s; T = 1.2 K. (A) 2QN–poly(dG·dC) complex; (B) 2QN–poly[d(G-C)$_2$] complex; (C) 2QN–poly[d(A-T)$_2$] complex; (D) 2QN–poly(dA·dT) complex; (E) 2QN–*E. coli* DNA complex. Concentrations of the 2QN–DNA complexes ranged from approximately 100 to 300 μM.

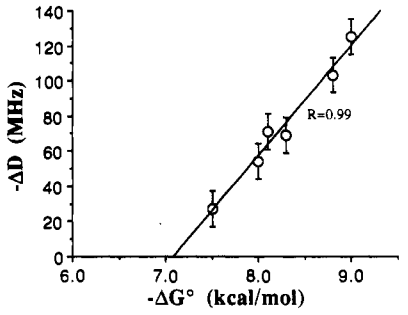

FIGURE 7: Plot of $-\Delta D$ versus $-\Delta G°$ for DNA complexes of 2QN. The ΔD values are from ODNR results of this work. The $\Delta G°$ values were calculated from independent 2QN equilibrium binding studies (Fox et al., 1980). The data included (in order of increasing $|\Delta G°|$) are for the 2QN complexes of *C. perfringens* DNA, calf thymus DNA, *M. lysodeikticus* DNA, *E. coli* DNA, poly[d(G-C)$_2$], and poly[d-(A-T)$_2$].

date. Field desorption mass spectrometry has been employed to characterize the molecular weight of the quinoline analogues of echinomycin (Bojesen et al., 1981). NMR investigations (Williamson et al., 1982) of the solution structure of the quinoline peptide have revealed evidence of only one conformation of the 2QN analogue in $CDCl_3$ similar to findings reported for echinomycin. HPLC investigations (Alfredson et al., 1990) of the quinoxaline and quinoline peptides have shown that both echinomycin and 1QN, the monosubstituted quinoline analogue of echinomycin, seem to be common contaminants in 2QN after biosynthetic workup but are easily removed by further chromatographic purification.

Wavelength-selected ODMR investigations of 2QN in LPSE buffer with 16% EG and methanol suggest that the peptide contains two distinct triplet states (blue and red triplet states) as evidenced by discontinuities in the plots of ODMR transition frequencies versus monitored emission wavelength and by the reversal of $D + E$ signal polarity in the ODMR spectra of 2QN as a function of emission wavelength in methanol. In aqueous buffer, the blue triplet state of 2QN has a zfs D parameter that is 53 MHz higher and an E parameter that is 22 MHz lower than the corresponding D and E parameters for the red triplet state of 2QN. The fact that, as was observed for echinomycin, each triplet state of the quinoline peptide is influenced independently in its interactions with nucleic acid targets further supports the existence of two distinct triplet states of the peptide under the conditions of this study. In other terms, plots of ODMR frequency vs emission wavelength of the nucleic acid complexes of 2QN revealed discontinuities similar to those of the free drug. As postulated for echinomycin, we think that a likely origin of the two triplet states of 2QN in aqueous and methanolic environments is the occurrence of two or more distinct conformations of the drug which bind differently to nucleic acid targets. One possibility is that more than one orientation of the quinoline rings relative to the peptide chain may exist in solution and lead to conformational isomers that are distinguishable at low temperatures and/or when a bisintercalation complex is formed.

Oligonucleotide–2QN Complexes. The binding of 2QN to the oligonucleotide duplexes d(ACGT)$_2$, d(TCGA)$_2$, and d-(ACGTACGT)$_2$ leads in each case to a red shift in the phosphorescence and a significant reduction in both D and E. These changes reflect in a qualitative manner the change in environment of the quinoline chromophores from the polar solvent to one that is more polarizable. These changes are consistent with the bisintercalative mode of binding which has been demonstrated using NMR for the parent antibiotic, echinomycin, binding to both tetranucleotides (Gao & Patel, 1988) and to the octanucleotide (Gilbert et al., 1989). Echinomycin binding to d(ACGT)$_2$ induces a Hoogsteen conformation for the A·T base pairs, whereas the A·T base pairs remain in a Watson–Crick conformation in the echinomycin–d(TCGA)$_2$ complex (Gao & Patel, 1988). Similar results have been obtained (Gilbert et al., 1989; Gilbert & Feigon, 1991) for the echinomycin complexes of d-(ACGTACGT)$_2$ and d(TCGATCGA)$_2$, which exhibit Hoogsteen base pairing of A·T (at low temperature) in the former and Watson–Crick pairing in the latter. Whether or not this is the case for the 2QN analogue, the stacking interactions should differ for the 2QN–d(ACGT)$_2$ and 2QN–d(TCGA)$_2$ complexes. The blue triplet state of each of these complexes retains the negative polarity ODMR signals of free 2QN, while there is a reversal of polarity of both the $2E$ and $D + E$ signal of the red triplet state. Although there is relatively little difference in the 2QN zfs between the two tetranucleotide complexes, the complexes with the octanucleotide produce a significantly larger ΔD (see Tables II and III), suggesting that the stacking interactions are larger in the latter complexes (see below). This suggests that the extent of these aromatic interactions depends upon the size of the oligonucleotide, in addition to the immediate binding site sequence.

Similar changes in signal polarity are observed when 2QN (see below) and echinomycin (Alfredson & Maki, 1990) bind to the natural DNAs. This effect is most likely the result of changes in the sublevel decay constants induced by the chromophore stacking interactions with DNA bases.

Polynucleotide–2QN Complexes. In contrast with oligonucleotide complexes, spectroscopic data and other structural information on polynucleotide–echinomycin complexes and their analogues are not available. Fluorescence titrations have been employed (Fox et al., 1980) to obtain the binding constants of 2QN with various synthetic polynucleotides and natural DNAs. As can be observed in Table V, the major (red) form of 2QN has the highest binding affinity to the alternating copolymers poly[d(A-T)$_2$] and poly[d(G-C)$_2$], while binding to the homopolymer duplexes is quite weak. A reversal of ODMR signal polarity is observed upon binding 2QN to each of the polynucleotides listed in Table V except for poly(dA·dT) which also shows negligible changes in the zfs. Thus, we do not think that a bisintercalation complex is formed with poly(dA·dT). Our results suggest intercalative complexing of 2QN with poly(dG·dC), although 2QN binding to this polynucleotide was not reported (Fox et al., 1980). Echinomycin, however, binds very tightly to poly(dG·dC) (Wakelin & Waring, 1974).

A reduction in the phosphorescence lifetime of the red triplet state, red shifts in phosphorescence emission maximum, decreases in the D values, and reversals in the $2E$ and $D + E$ signals in the ODMR spectrum of the red triplet state upon binding are shared features of the oligomeric and natural DNA complexes. The similarity of results obtained for the 2QN–d(ACGTACGT)$_2$ and the 2QN complexes with *M. lysodeikticus* and *E. coli* DNA is very striking, suggesting that the oligonucleotide serves as a good model for the majoriy binding sites in the latter. This is in marked contrast to the interactions of the d(ACGTACGT)$_2$ target with echinomycin, the parent antibiotic of 2QN, which strongly resemble those of the antibiotic–poly[d(A-T)$_2$] complex and suggested that interactions of the quinoxaline rings with A·T base pairs flanking the bisintercalation site were responsible for the changes observed in triplet-state properties of the chromophores (Alfredson & Maki, 1990).

Among the 2QN–polymeric DNA complexes examined in this report, a comparison of the results obtained with the synthetic polymers with the results obtained with the native DNAs is quite revealing. Although 2QN has the highest binding affinity to poly[d(A-T)$_2$] and poly[d(G-C)$_2$] among the DNA polymers studied in this report, the changes in triplet-state properties of 2QN upon binding to these targets do not resemble those of the natural DNAs. Binding to these synthetic DNA polymers results in a larger reduction in D, but a smaller reduction in E relative to the native DNAs. 2QN displays very insignificant changes in triplet-state properties upon binding to poly(dA·dT), which suggests a weak interaction of the peptide with this nucleic acid target (a trait shared by echinomycin).

The polarity reversal of the signals observed in the ODMR spectra of the red triplet state of 2QN reflects relative steady-state population shifts of the individual triplet sublevels induced upon binding to the DNAs. Measurements of the sublevel decay rate constants for the red triplet state of 2QN reveal a consistent trend in the changes observed upon 2QN binding to the natural DNAs and alternating copolymers that is not observed in the 2QN–poly(dA·dT) complex. A significant increase in the decay rate constant is noticed for the radiative T_z sublevel upon complexation to these DNA targets while the other sublevel decay constants decrease slightly. This same trend was observed for echinomycin upon binding to the polynucleotides found to induce signal inversion upon complex formation. This pattern also is mirrored by changing quinoline from a polar to nonpolar solvent (see Table VI). As is the case for quinoxaline, the increase in the T_z decay constant is a consequence of enhanced spin–orbit coupling in nonpolar solvents (van der Waals & de Groot, 1967).

The reduction of the zfs D parameter ($-\Delta D$) of the red triplet state of 2QN upon binding to the DNA polymers appears to be directly related to the binding affinity of these nucleic acid targets (see Table V). The reduction in the D value is expected to increase with the extent of aromatic stacking interactions involving the peptide chromophore on the basis of previous studies of Lys-Trp-Lys complex formation with poly(dT) (Maki & Cha, 1983). The size of the $-\Delta D$ values exhibited by the quinoline chromophores of the 2QN–polynucleotide complexes is of the same order of magnitude as those previously reported for stacking interactions between Trp residues and nucleoide bases in the binding of *E. coli* single-stranded DNA binding proteins and poly(dT) (Khamis et al., 1987) and those measured for cyclophanes in which naphthalene rings (approximately 3.1 Å apart) are forced into stacking arrangements by out-of-plane methylene bridges (Haenel & Schweitzer, 1988). Both proximity and orientation of the interacting ring systems were found to influence the magnitude of the reduction of the zfs D parameter of the phanes relative to their monomeric units.

Linear Dependence of ΔD on $\Delta G°$. The linear relationship between ΔD, a property of the excited triplet state of the intercalated chromophore, and $\Delta G°$, a ground electronic state property of the entire complex, is convincingly demonstrated in Figure 7. It is not obvious that there should be any relationship between these quantities, one being spectroscopic and the other thermodynamic. An explanation is suggested by measurements that have been made (von Schütz et al., 1974; van Egmond et al., 1975; Kwiram et al., 1978) on the relationship between the zfs and the solvent shift of the triplet electronic energy, ΔE_{ST}. When the zfs D parameter is plotted against the solvent shift monitored by narrow-band optical detection through the inhomogeneously broadened phosphorescence 0,0-band, a linear relationship is found. For quinoxaline in 3-methylpentane, for example, $\Delta(D + E)/\Delta E_{ST} = +6 \times 10^{-6}$ (Gradl et al., 1986); i.e., the zfs decreases as the 0,0-band phosphorescence is monitored at increasing wavelengths. For quinoxaline in LPSE buffer containing 16% (v/v) ethylene glycol we find (Alfredson & Maki, 1990) $\Delta(D + E)/\Delta E_{ST} = 7 \times 10^{-6}$. Since the change in zfs E parameter (ΔE) is linear with respect to ΔE_{ST}, $\Delta D/\Delta E_{ST}$ is constant and equal to $+6.5 \times 10^{-6}$. From Figure 3, we obtain $\Delta D/\Delta E_{ST} = +5.7 \times 10^{-6}$ for quinoline in LPSE buffer containing 16% (v/v) ethylene glycol. Furthermore, $\Delta D/\Delta E_{ST} = +7.5 \times 10^{-6}$ for the red triplet state of 2QN in the same solvent, while for echinomycin this slope is slightly less, $+6.5 \times 10^{-6}$ (Alfredson & Maki, 1990), the same value as for quinoxaline. The correlation between the shift in the zfs and ΔE_{ST} suggests that these perturbations have a common origin. An explanation (Lemaistre & Zewail, 1979) based on a model in which the zfs inhomogeneity was directly related to the optical inhomogeneity via the intramolecular spin–orbit coupling was shown (Gradl & Friedrich, 1985) to be applicable only to molecules that are subject to large internal or external heavy atom effects. Specifically, the Lemaistre and Zewail model does not apply to molecules such as quinoline or quinoxaline. An alternate model, first suggested by van Egmond et al.

(1975), and subsequently refined (Gradl & Friedrich, 1985; Gradl et al., 1986; Williamson & Kwiram, 1988), employs the solvent-induced mixing of excited molecular triplet states with the phosphorescent state. This is effectively a solvent-produced Stark perturbation which only can cause mixing of states having the same spin multiplicity. The mixing of excited triplet states with the phosphorescent T_1 state lowers its energy and causes a concomitant change in the electronic wave function which in turn perturbs the zfs. The model predicts a linear dependence of the zfs on the solvent-induced Stark shift in agreement with observations. The magnitude of $\Delta D/\Delta E_{ST}$ is predicted to be relatively invariant and given by

$$\frac{E_{zfs}}{E_{TT}} \sim \frac{0.1\ \text{cm}^{-1}}{10000\ \text{cm}^{-1}} = 10^{-5} \tag{1}$$

where E_{zfs} is the zero-field splitting energy and E_{TT} refers to the energy separation between T_1 and a typical admixed higher energy triplet state. The magnitude predicted for E_{zfs}/E_{TT} is in agreement with the measurements quoted above. A positive sign for $\Delta D/\Delta E_{ST}$ is predicted if (a) the magnitude of the zfs of the higher energy admixed triplet states (generally assumed to be more diffuse, according to theory) is smaller than that of T_1 and (b) the solvent effect is ignored for the ground state, S_0, which usually is assumed to be less polarizable than T_1. Although this model neglects the solvent perturbation of the S_0 energy, the predicted sign of $\Delta D/\Delta E_{ST}$ also would be positive provided a S_0 energy perturbation were smaller than that of T_1. We suggest that the correlation between the zfs and $\Delta G°$ observed in 2QN as well as in echinomycin (Alfredson & Maki, 1990) implies that the stacking interactions in the peptide–DNA complex lower the ground-state energy of the intercalated aromatic residue; this reduced ground-state energy shows up as a contribution to $\Delta G°$ of the complex. The neglect of a solvent perturbation on the S_0 energy in the previous model (van Egmond et al., 1975; Gradl & Friedrich, 1985; Gradl et al., 1986) is not always justified in our view; no correlation between the zfs and the ground-state energy would be predicted by this model, only a correlation between the zfs and E_{ST} based on altered properties of the T_1 state, alone. In support of the suggestion that ground-state energy perturbations are important, recent work (Ghosh et al., 1988) on metal ion binding to naphthalene crown ethers, in which closed shell metal ions were introduced along the *x*-, *y*-, and *z*-axes (long-in-plane, short-in-plane, and out-of-plane axes, respectively) of the naphthalene chromophore, showed that binding along *x* and *y* led to red and blue shifts of E_{ST}, respectively. Since naphthalene is nonpolar in both the S_0 and T_1 states and thus should have a negligible first-order Stark shift, the blue shift of E_{ST} for *y*-axis metal ion binding suggests a larger second-order Stark shift of the S_0 energy than of the T_1 energy. (Second-order Stark shifts of S_0 and T_1 energies are always negative.)

Modified Solvent Effect Theory. We adopt a perturbation theory model analogous to that of van Egmond et al. (1975) but now allow for the perturbation of the ground singlet energy by an effective solvation Hamiltonian which acts only on the spatial coordinates of the composite particles of the aromatic molecule.

We will call ψ^0_{ir} ($i = 1, 2, ..., j, ...; r = x, y, z$) the triplet-state eigenfunctions of the molecule in the solvent environment represented by the Hamiltonian, H_0, while Φ^0_m ($m = 0, 1, 2, ..., n, ...$) are the corresponding singlet eigenfunctions. The indexes *i* and *m* increase in order of increasing electronic energy, so that Φ^0_0 and ψ^0_{1r} are the ground electronic state and phosphorescent state, respectively, in the solvent environment. When the chromophore interacts with DNA, its new environment is represented by the Hamiltonian H_c, such that

$$H_c = H_0 + H_s \tag{2}$$

where H_s represents the effect of base stacking interactions. We then use H_s as a perturbation in the basis of H_0 and obtain expressions for the effects of complexation on the ground- and phosphorescent-state energies, as well as on the zfs. The appropriate expressions for the electronic energy perturbations are

$$\Delta E_0 = \langle \Phi^0_0|H_s|\Phi^0_0\rangle + \sum_n \frac{[\langle \Phi^0_n|H_s|\Phi^0_0\rangle]^2}{\Delta_{0n}} \tag{3}$$

and

$$\Delta E_{1r} = \langle \psi^0_{1r}|H_s|\psi^0_{1r}\rangle + \sum_j \frac{[\langle \psi^0_{jr}|H_s|\psi^0_{1r}\rangle]^2}{\Delta_{1r,jr}} \tag{4}$$

where ΔE_0 and ΔE_{1r} are shifts of the S_0 and T_1 states, respectively, given to second order. In these expressions, *n* and *j* label singlet and triplet excited states, respectively, and

$$\Delta_{0n} = E^0_0 - E^0_n \tag{5}$$

and

$$\Delta_{1r,jr} = E^0_1 + \epsilon^0_{1r} - (E^0_j + \epsilon^0_{jr}) \tag{6}$$

where the E^0 refer to the zero-order electronic energy eigenvalues and ϵ^0_{kr} is the zf energy of the τ_r magnetic sublevel of the ψ^0_k state. We ignore the first term on the right-hand side of the eqs 3 and 4, which is expected to be small since the molecule is essentially nonpolar in both the Φ^0_0 and ψ^0_1 (π,π^*) state. Furthermore, we assume as in previous work (van Egmond et al., 1975; Gradl & Friedrich, 1985; Gradl et al., 1986) that ψ^0_{1r} is coupled predominantly to a single excited triplet state by H_s and that a similar restriction applies to Φ^0_0. Equations 3 and 4 then simplify to

$$\Delta E_0 = \frac{[\langle \Phi^0_n|H_s|\Phi^0_0\rangle]^2}{\Delta_{0n}} \tag{7}$$

and

$$\Delta E_{1r} = \frac{[\langle \psi^0_j|H_s|\psi^0_1\rangle]^2}{\Delta_{1r,jr}} \tag{8}$$

where we have omitted the *r* designation in the matrix element of eq 8, since it is independent of the spin sublevel.

We can obtain the effect of H_s on the zfs by using eq 8 with $r = v$ and $r = u$, and subtracting the two expressions. This gives

$$\Delta\epsilon_{vu} = \frac{[\langle \psi^0_j|H_s|\psi^0_1\rangle]^2}{\Delta_{1j}^2}(\epsilon^0_{j,vu} - \epsilon^0_{1,vu}) \tag{9}$$

where $\Delta\epsilon_{vu}$ is the change in the energy separation between the τ_v and τ_u sublevels of the ψ_1 state while $\epsilon^0_{j,vu} = (\epsilon^0_{jv} - \epsilon^0_{ju})$, etc. For convenience, we choose *v* and *u* such that $\epsilon^0_{1,vu}$ is positive. In the previous model which ignores the solvent effect on the ground-state energy, $\Delta E_0 = 0$, and ΔE_1 can be identified with ΔE_{ST}, the shift in the phosphorescence energy. This approximation gives (dividing eq 9 by eq 8)

$$\frac{\Delta\epsilon_{vu}}{\Delta E_1} = \frac{(\epsilon^0_{j,vu} - \epsilon^0_{1,vu})}{\Delta_{1j}} \tag{10}$$

Since Δ_{1j} is negative, this quantity is positive if $\epsilon^0_{1,vu} > \epsilon^0_{j,vu}$, which is often assumed. What we are actually interested in is the relationship between $\Delta\epsilon_{vu}$ and ΔE_{ST}, and later, with ΔE_0. Since

$$\Delta E_{ST} = \Delta E_1 - \Delta E_0 \quad (11)$$

combining eqs 7 and 8 (neglecting the zf energy relative to the electronic energy) gives

$$\Delta E_{ST} = \Delta E_1(1 - q) \quad (12)$$

where

$$q = \frac{[\langle \Phi_n^0 | H_s | \Phi_0^0 \rangle]^2}{[\langle \psi_j^0 | H_s | \psi_1^0 \rangle]^2}\left(\frac{\Delta_{1j}}{\Delta_{0n}}\right) \quad (13)$$

Note that $q \geq 0$. Then, combining eqs 10 and 12

$$\frac{\Delta\epsilon_{vu}}{\Delta E_{ST}} = \frac{(\epsilon_{j,vu}^0 - \epsilon_{1,vu}^0)}{\Delta_{1j}(1 - q)} \quad (14)$$

This is the quantity which experimental evidence indicates is a constant. If $q = 0$, eq 14 reduces to that of the original theory (eq 10) in agreement with experimental evidence. If $q > 0$, agreement with experimental observations requires that q be independent of variations in H_s, i.e., differences in solvation or DNA intercalation sites. This, in turn, requires that the matrix elements of eq 13 change proportionally with any changes in H_s so that their ratio remains the same. Here we have arrived at a critical point in the analysis; the invariance of this ratio to small changes in H_s appears reasonable considering that Φ_0^0 and ψ_1^0 differ principally by the π–π^* excitation of a single electron. We expect that q should be largely a property of the aromatic molecule, at least for relatively small variations in H_s which might characterize differing DNA binding sites.

Equations 10–12 give

$$\frac{\Delta\epsilon_{vu}}{\Delta E_0} = \frac{(\epsilon_{j,vu}^0 - \epsilon_{1,vu}^0)}{q\Delta_{1j}} \quad (15)$$

Thus, the ratio of the zfs change to the change in ground-state energy of the chromophore resulting from DNA binding is constant, provided that q does not vary with binding site, as discussed above. Equation 15 provides a rationale for the observed linear relationship between the zfs and $\Delta G°$ for 2QN complexing with the various DNAs examined in this paper. Since entropic contributions to the binding free energy are expected to be reasonably independent of the specific intercalation site in a bisintercalation complex of 2QN, we can assume that the ΔE_0 can be taken as the contribution per intercalated molecule to the free energy of binding. This contribution arises largely from the dispersive type of interactions discussed here. It is of interest to note that for 2QN the magnitude of $\Delta D/\Delta G°$ obtained from Figure 7 is $+5.9 \times 10^{-6}$, while $\Delta D/\Delta E_{ST}$ obtained from Figure 3 is $+7.5 \times 10^{-6}$. There are two intercalating residues in the drug molecule; thus $\Delta G° \sim 2\Delta E_0$, and $\Delta D/\Delta E_0 \sim +1.2 \times 10^{-5}$. Since the sign of this quantity is the same as that of $\Delta D/\Delta E_{ST}$, comparison of eqs 14 and 15 suggests that $q < 1$. This limit is quite reasonable from eq 13 if the sizes of the H_s matrix elements are not very different. In fact, these slopes are consistent for $q \sim 0.38$, which is quite reasonable.

One important conclusion that can be drawn is that since the data for 2QN binding to different DNA sequences fall on a single regression line (Figure 7), the peptide contribution to the binding free energy must be independent to a large extent of the sequence of the DNA binding site. Thus, the van der Waals contacts and hydrogen-bonding interactions of the peptide such as those observed in the X-ray crystal structure of a specific complex of echinomycin with the duplex $d(CGTACG)_2$ (Ughetto et al., 1985) must be largely self-compensating as the base sequence is varied. The structure of echinomycin with its extensive peptide methylation is expected to limit hydrogen-bonding possibilities with DNA bases in the binding site. Our results appear to point to the conclusion that in 2QN (and in 1QN and echinomycin; unpublished results) the sequence specificity of the drugs rests largely in the aromatic stacking interactions. For 2QN, the peptide contribution to $\Delta G°$ is ca. −7 kcal/mol (Figure 7), while the range of aromatic stacking contributions is about −2 kcal/mol or −1 kcal/mol of intercalated residues, which is a reasonable magnitude for these interactions (Borer et al., 1975).

Although the binding of 2QN to the homopolymer duplexes poly(dA·dT) and poly(dG·dC) has not been quantitatively evaluated (Fox et al., 1980), our ODMR measurements (Table V) and the regression established in Figure 7 allow the prediction that $K_0 < 0.16 \times 10^6$ and $K_0 \sim 2.5 \times 10^6$ for the complexes 2QN–poly(dA·dT) and 2QN–poly(dG·dC), respectively.

It is interesting that when H_s represents the effect of base stacking interactions on the electronic states of the intercalator, it is only the zfs D parameter which plots linearly against $\Delta G°$. Analogous plots of $D + E$ vs $\Delta G°$ show little correlation. This is not the case for general solvent effects where both D and E correlate well with ΔE_{ST}, as discussed earlier. We believe that these differences arise because the aromatic stacking interactions are highly directional [largely affecting the electron delocalization along the stacking axis, to which D is particularly sensitive (McGlynn et al., 1969)] while the general solvent effects are more nearly isotropic, affecting the D and E parameters proportionally.

References

Alfredson, T. V., & Maki, A. H. (1990) *Biochemistry 29*, 9052–9064.

Alfredson, T. V., Maki, A. H., Adaskaveg, M. E., Excoffier, J.-L., & Waring, M. J. (1990) *J. Chromatogr. 507*, 277–292.

Bojesen, G., Gauvreau, D., Williams, D. H., & Waring, M. J. (1981) *J. Chem. Soc., Chem. Commun. 10*, 46–47.

Borer, P. N., Dengler, B., & Tinoco, I., Jr. (1974) *J. Mol. Biol. 86*, 843–853.

Cornish, A., Fox, K. R., & Waring, M. J. (1983) *Antimicrob. Agents Chemother. 23*, 221–228.

Fox, K. R., Gauvreau, D., Goodwin, D. C., & Waring, M. J. (1980) *Biochem. J. 191*, 729–736.

Gao, X., & Patel, D. J. (1988) *Biochemistry 27*, 1744–1751.

Gauvreau, D., & Waring, M. J. (1984) *Can. J. Microbiol. 30*, 439–451.

Ghosh, S., Petrin, M., & Maki, A. H. (1988) *J. Chem. Phys. 88*, 2913–2918.

Gilbert, D. E., & Feigon, J. (1991) *Biochemistry 30*, 2483–2494.

Gilbert, D. E., van der Marel, G. A., van Boom, J. H., & Feigon, J. (1989) *Proc. Natl. Acad. Sci. U.S.A. 86*, 3006–3010.

Gradl, G., & Friedrich, J. (1985) *Chem. Phys. Lett. 114*, 543–546.

Gradl, G., Friedrich, J., & Kohler, B. E. (1986) *J. Chem. Phys. 84*, 2079–2083.

Haenel, M. W., & Schweitzer, D. (1988) *Adv. Chem. Ser. 217*, 333–355.

Khamis, M. I., Casas-Finet, J. R., Maki, A. H., Murphy, J. B., & Chase, J. W. (1987) *J. Biol. Chem. 262*, 10938–10945.

Kwiram, A. L., Ross, J. B. A., & Deranleau, D. A. (1978) *Chem. Phys. Lett. 54*, 506–509.

Lee, J. S., & Waring, M. J. (1978) *Biochem. J. 173*, 115–128.

Low, C. M. L., Drew, H. R., & Waring, M. J. (1984) *Nucleic Acids Res. 12*, 4865–4879.
Maki, A. H., & Co, T. (1976) *Biochemistry 15*, 1229–1235.
Maki, A. H., & Cha, T.-A. (1983) *Photochem. Photobiol. 2*, 1035–1055.
McGlynn, S. P., Azumi, T., & Kinoshita, M. (1969) *Molecular Spectroscopy of the Triplet State*, p 99, Prentice-Hall, Englewood Cliffs, NJ.
Quigley, G. J., Ughetto, G., van der Marel, G. A., van Boom, J. H., Wang, A. H.-J., & Rich, A. (1986) *Science 232*, 1255–1261.
Schmidt, J., Antheunis, D. A., & van der Waals, J. H. (1971) *Mol. Phys. 22*, 1–17.
Tsao, D. H. H., Casas-Finet, J. R., Maki, A. H., & Chase, J. W. (1989) *Biophys. J. 55*, 927–936.
Ughetto, G., Wang, A. H.-J., Quigley, G. J., van der Marel, G. A., van Boom, J. H., & Rich, A. (1985) *Nucleic Acids Res. 13*, 2305–2323.
van der Waals, J. H., & de Groot, M. S. (1967) *Magnetic Interactions Related to Phosphorescence*, in *The Triplet State* (Zahlan, A. B., Ed.) pp 101–132, Cambridge University Press, Cambridge.
Van Dyke, M. M., & Dervan, P. B. (1984) *Science 225*, 1122–1127.
van Egmond, J., Kohler, B. E., & Chan, I. Y. (1975) *Chem. Phys. Lett. 34*, 423–426.
Vincent, J. S., & Maki, A. H. (1965) *J. Chem. Phys. 42*, 865–868.
von Schütz, J. U., Zuclich, J., & Maki, A. H. (1974) *J. Am. Chem. Soc. 96*, 714–718.
Wakelin, L. P. G. (1986) *Med. Res. Rev. 6*, 275–340.
Wakelin, L. P. G., & Waring, M. J. (1976) *Biochem. J. 157*, 721–740.
Wang, A. H.-J., Ughetto, G., Quigley, G. J., Hakoshima, T., van der Marel, G. A., van Boom, J. H., & Rich, A. (1984) *Science 225*, 1115–1121.
Waring, M. J., & Wakelin, L. P. G. (1974) *Nature 252*, 653–659.
Williamson, M. P., Gauvreau, D., Williams, D. H., & Waring, M. J. (1982) *J. Antibiot. 35*, 62–66.
Yoshida, T., Kimura, Y., & Katagiri, K. (1968) *J. Antibiot. 7*, 465–467.

Structure of Colorado Potato Beetle Lipophorin: Differential Scanning Calorimetric and Small-Angle X-ray Scattering Studies†

Chihiro Katagiri,*,‡ Mamoru Sato,§ Stan de Kort,‖ and Yukiteru Katsube§

Biochemistry Laboratory, Institute of Low Temperature Science, Hokkaido University, Sapporo, Japan, Institute for Protein Research, Osaka University, Suita, Japan, and Department of Entomology, Agricultural University, Wageningen, The Netherlands

Received February 28, 1991; Revised Manuscript Received June 26, 1991

ABSTRACT: The structure of lipophorin, isolated from hemolymph of the Colorado potato beetle, was investigated by differential scanning calorimetry (DSC) and small-angle X-ray scattering. The DSC heating curves of intact lipophorin showed endothermic peaks that were similar to peaks obtained with the hydrocarbon fraction isolated from this lipophorin. The observed peaks correlated with the transition of the hydrocarbons from an ordered into a more disordered state. Changes in structure of the lipophorin particles with increasing temperature were also observed by small-angle X-ray scattering studies. The structural organization of lipophorin was further elucidated by simulation analysis, using a three-layered symmetrical sphere as a model. These studies revealed that lipophorin from the Colorado potato beetle is a sphere with a maximum diameter of 175 Å. The sphere is composed of three radially symmetrical layers of different electron densities. The outer layer (37.5–39.5 Å in thickness) is composed of phospholipid, apolipophorin I, and part of apolipophorin II. The middle layer (5–10 Å) contains diacylglycerol, the rest of apolipophorin II, and probably β-carotene. The core of the particle (40–45 Å) only contains hydrocarbons. This structure differs from another model, previously proposed for cockroach and locust lipophorins [Katagiri, C., Sato, M., & Tanaka N. (1987) *J. Biol. Chem. 262*, 15857–15861], in the small size of the middle layer. The volume of the middle layer correlated well with the low diacylglycerol content of this lipophorin.

Since lipids are not water soluble, lipoproteins are essential for transport within animals from the sites of synthesis, absorption, and storage to sites of utilization (Chino, 1985; Goldstein et al., 1985; Shapiro et al., 1988). Lipoproteins from different animals have basically a common molecular architecture. The surface is covered with hydrophilic groups of phospholipids and apoproteins, whereas the core contains apolar lipids (Edelstein et al., 1979; Katagiri et al., 1987). Despite the common structural organization, lipoproteins may vary in physiological function, chemical composition, and metabolism. Mammalian lipoproteins, classified by their buoyant density, transport mainly triacylglycerol and cholesterol esters and are metabolized in peripheral cells and liver (Goldstein et al., 1985). In insects, a circulating lipoprotein, named lipophorin, transports diacylglycerol, free cholesterol, and hydrocarbons. Phospholipids, a major lipid class in insect

† This work was supported in part by a research grant (01540586) from the Ministry of Education, Science and Culture of Japan.
* To whom correspondence should be addressed.
‡ Hokkaido University.
§ Osaka University.
‖ Agricultural University.

0006-2960/91/0430-9675$02.50/0